Scanning Microscopy

Volume 2 | Number 4 Article 12

9-8-1988

Contrast and Resolution of Secondary Electron Images in a Scanning Transmission Electron Microscope

J. Liu
Arizona State University

J. M. Cowley
Arizona State University

Scanning Microscopy, Vol. 2, No. 4, 1988 (Pages 1957-1970)
Scanning Microscopy International, Chicago (AMF O'Hare), IL 60666 USA

0891-7035/88$3.00+.00

CONTRAST AND RESOLUTION OF SECONDARY ELECTRON IMAGES IN A SCANNING TRANSMISSION ELECTRON MICROSCOPE

J. Liu and J. M. Cowley*

Department of Physics
Arizona State University, Tempe, AZ 85287 USA

(Received for publication February 26, 1988, and in revised form September 08, 1988)

Abstract

Recent advances in the improvement of secondary electron image resolution to the subnanometer level demand further knowledge of the origin of secondary electron emission to interpret the experimental results. The generally accepted estimation of the non-localized range of the inelastic scattering of incident electrons and the subsequent generation of secondary electrons in a solid cannot explain the 0.7 nm resolution of secondary electron images obtained in a scanning transmission electron microscope operated at 100 kV. Resolution and contrast of secondary electron images are interrelated. High contrast as well as high resolution can be obtained at the same time. Contrast mechanisms are also complicated due to the origin of the generation of secondary electrons by incident electrons or by other energetic secondary electrons. Surface adsorption and thin layer contamination will change the collected secondary electron signal dramatically which makes the image interpretation difficult. Surface defects might give observable secondary electron image contrast due to the change of total secondary electron yield caused by the defects or by the adsorbed species at the defect. Ultra-high resolution secondary electron imaging provides important information in the study of surface reactions and related surface problems in a scanning transmission electron microscopy instrument.

Key Words: High resolution secondary electron imaging, inelastic scattering, localization, channeling effect, "cascade" electrons, "coherent" secondary electrons.

* **Address For Correspondence:**
J. M. Cowley, Department of Physics
Arizona State University, Tempe, AZ 85287
Phone No:(602) 965-6459

Introduction

In recent years, ultra-high resolution secondary electron imaging has been made possible by incorporating a field emission gun and by putting the specimen inside the highly excited objective pole-pieces in a scanning electron microscope [29-30, 33-34, 53-54]. Nagatani and Saito [33] have claimed a resolution of 0.8 nm (point resolution) with their FESEM operated at 30 kV. Tanaka et al [53] have demonstrated approximately 0.5 nm resolution on a biological specimen and Kuroda et al [29-30] have resolved 0.45 nm high atomic steps of 1.4 nm periodicity on a tungsten emitter sample. In a scanning transmission electron microscope (STEM) the secondary electron signals are detected at the exit surface of the sample as described by Imeson et al [23]. The absence of the contribution from the type II secondary electrons (generated by backscattered electrons) to the total detected signals and the fact that very thin specimens are usually used in STEM research work make ultra-high resolution secondary electron imaging (in transmission mode) possible in a STEM instrument. Furthermore, with this detection configuration it is possible to investigate the SE image intensity variation with specimen thickness, which may yield more information about the origin of SE emission [32].

It has been reported [13] that with an electron microscope operated at 100 kV the ultimate resolution limit of secondary electron images cannot be better than 1 nm, even with a point source probe, due to the intrinsic non-localized nature of the inelastic scattering processes involved in generating secondary electrons in a solid. Yet, subnanometer resolution of secondary electron images has been obtained experimentally in a 100 kV STEM instrument with a probe diameter of 0.5 nm under normal operating conditions. A preliminary survey of the imaging condition and various contrast mechanisms of SE images obtainable in a STEM instrument, along with possible applications of this imaging mode, has been previously reported [31-32]. In this paper a resolution of 0.7 nm of SE images, obtained with a 100 kV electron microscope with a probe diameter of about 0.5 nm or less, will be demonstrated.

All these new experimental results demand further understanding of the physics of SE emission. More investigation is needed to understand the image contrast (e.g., atomic step contrast) as well as the ultimate resolution limit imposed by the non-localized inelastic scattering processes governing the spatial distribution of the generated secondary electrons.

The physics of secondary electron emission becomes

more and more important for the SE imaging theory as the resolution improves to subnanometers. "Cascade electrons" have been studied by various methods (e.g., Boltzmann equation method, Monte Carlo simulation, etc.) for a long time. "Coherent" secondary electrons (defined in the next section) carry information about the band structure of the material studied. These electrons are high resolution imaging signals and for very thin specimens they may play an important role for image formation as compared with the cascade electrons. With energy analysis of the emitted secondary electrons it might be possible to extract information about the band structure of the bulk material as well as the influence of the surface on the energy bands from these coherently emitted secondary electrons for very thin specimens.

The interpretation of SE images has always been complicated by the presence of adsorbed species and contamination on specimen surfaces. The fact that SE signals are very sensitive to surface modifications (electronic and geometric) makes this imaging mode a unique one to provide surface information as compared with other imaging and diffraction modes in a STEM instrument. Surface and subsurface defects may change the generation of SE signals [35]. Thus, it might be possible to image surface defects by collecting SE signals. One complication is again the preferential adsorption of other species on the surface defects which will also change the detected SE signals significantly.

Origin of Secondary Electrons

Since the discovery of SE emission in 1902 by Austin and Starke [1], numerous theoretical as well as experimental investigations of the emission theory have been performed and great progress has been made as evidenced by the large number of research and review papers on this subject [4-10, 14, 16-17, 25, 35, 40-41, 43-47, 52]. Yet, the theory of SE emission still needs to be investigated in order to explain recent experimental results. The complexity of the generation processes and the subsequent transportation to specimen surfaces make it difficult to find an adequate theory to explain various experimental results. Furthermore even the basic physics of the generation mechanism of secondary electrons is not clearly understood. The problem concerning the lateral spatial distribution of the generated secondary electrons at the exit surface, which is related to the localization of the inelastic scattering processes involved in the production of secondary electrons, has not been fully discussed in the literature. This problem plays a minor role for low resolution SE images. But it is crucial to the understanding of the ultimate resolution limit of secondary electron images which we will discuss in the next section.

In electron microscopes incident electrons can be scattered both elastically and inelastically by the specimen. While elastic scattering yields important information on the specimen atomic structure, inelastic scattering gives information about the electronic structure of the studied material. Energy as well as momentum transfer from incident electrons to specimen electrons occur through inelastic scattering. Various specimen-specific signals can be generated at the site where an inelastic scattering event happens [39]. The detection of these signals provides a variety of information for characterizing specimen properties. Secondary electrons, arbitrarily defined in the literature as those emitted with energies less than 50 eV, are one product of this process. In the following, secondary electrons are referred to as those specimen electrons which have acquired enough energy to overcome the specimen surface barrier, represented by the work function of the sample, from the incident electrons.

Electrons inside a solid can be described by Bloch wave functions. The inner shell electrons are considered to be localized at the atomic sites while the valence electrons can move more freely. Band theory is needed to describe the energy distribution of these electrons. The so-called secondary electrons are in fact those specimen electrons which have been excited to higher energy states by the incident electrons or by other energy transfer processes. Thus the band structure and the density of states will impose some restrictions on the energy distribution of the generated secondary electrons (e.g., for insulators with large energy gaps between conduction and valence bands any excited state has energy higher than the vacuum level while the situation is quite different for metals). The excited Bloch electrons can interact with other specimen electrons to generate more excited electrons with lower energies. The Bloch states are not independent of each other. They interact to generate new Bloch states. Near the specimen surface the excited electrons can also be emitted into vacuum provided that the energy corresponding to that part of the momentum which is perpendicular to the specimen surface is higher than the specimen work function and the generalized momentum conservation law is obeyed:

$$\mathbf{K}||^{out} = \mathbf{K}||^{in} + \mathbf{G} \qquad (1)$$

where $\mathbf{K}||^{out}$ and $\mathbf{K}||^{in}$ are the tangential components of the wave vectors of the emitted secondaries outside and inside the specimen surface, respectively, and $\mathbf{G}$ is a reciprocal lattice vector.

The generation of secondary electrons is the least understood step of the emission theory. The probability of the excitation of inner shell electrons can be calculated quantum mechanically by assuming a single electron excitation model since these electrons are considered to be localized at the atomic sites. The excitation of valence electrons is more complicated. These electrons are initially less localized and they have to be described by Bloch wave functions rather than by localized atomic wave functions. High energy secondary electrons ($E > 100$ eV) are generated by single electron excitations. Low energy secondary electrons ($E < 50$ eV) can be generated by single electron excitations as well as by collective excitations through an indirect excitation-decay process: incident electron ⇒ plasmon ⇒ secondary electron. This is an indirect non-localized excitation-decay process. Bindi et al [4, 5] have included the volume plasmon decay as a source of generating secondary electrons in their calculation of secondary electron emission by the transportation method. A related problem is the production of secondary electrons by the surface plasmon excitation-decay process. In view of the fact that the collected secondary electrons come only within a thin region near the specimen surface this latter process may play a more significant role than the volume plasmon decay does. On the other hand, surface plasmon has a lower excitation energy than volume plasmon does. Hence, it may be possible that the secondary electrons generated through this process do not obtain enough energy to overcome the surface barrier for some materials (e.g., some insulators). For other cases, the low energy secondary electrons have a low transmission

probability through the solid-vacuum interface. Thus whether the surface plasmon excitation-decay process plays a significant role in the emission of secondary electrons depends on the specific material studied.

Another model of generating secondary electrons, which might not be negligible for semiconductor and insulator materials, is the exciton excitation-decay process. Incident electrons can generate excitons with energies above the vacuum level. These excitons can be described by Bloch wave functions or alternatively by the superposition of localized Wannier functions. The existence of these exciton energy levels will influence the inelastic excitation processes and subsequently the inner energy distribution of the generated secondary electrons. These excitons may decay by emission of light quanta or by generation of hot secondary electrons.

The probability of each excitation process depends on the specific material studied. The various kinds of excitations can be initiated by incident electrons as well as by other energetic secondary electrons (e.g., ionized inner shell electrons, Auger electrons, etc.). Although the probability of generating high energy secondary electrons is relatively small compared with the probability of low energy valence electron excitations by incident electrons, the subsequent excitation of valence electrons by these energetic secondary electrons (E =50 - 2000 eV) may give a probability of generating low energy secondary electrons 50 to 100 times higher than that for generation directly by 100 kV electrons. The energetic secondary electrons can escape from the specimen with a large escape depth. Thus the low energy secondary electron intensity generated by these indirect processes may be comparable to that directly produced by incident electrons near the specimen surface. In view of this, we know that the original excitation event (or stated in another way, the information depth) may be far inside the bulk sample although the collected secondary electrons originate from only 1 to 5 nm inside the surface.

The secondary electrons generated through collective excitations (e.g., plasmons, excitons, etc.) in large crystals are not high resolution signals although they will influence the contrast of the SE images of thick specimens. For ultra-high resolution secondary electron imaging these signals will contribute a spatially extended background to the image intensity, lowering the contrast and the resolution of the SE image.

However, those secondary electrons, which are generated within a transition region near the solid-vacuum interface (in accordance with different inelastic mean free paths of secondary electrons with different energies) by incident electrons, contain ultra-high resolution signals. Those hot secondary electrons have suffered no inelastic collisions before they escape. The generation probability of these secondary electrons is directly related to the joint density of the initial and final states of the Bloch electrons within the surface region. These secondary electrons carry information about the band structure of the studied material and they are emitted directly from the excited Bloch states. The so emitted secondary electrons are called coherent secondary electrons in this sense [27-28].

All secondary electrons have to overcome the surface barrier to be emitted into vacuum. This imposes further restriction on the low energy secondary electrons. For metals most of the excited electrons cannot be emitted since they have energies lower than the work function. For large band gap insulators nearly all of the excited electrons can be emitted into the vacuum since they have energies higher than the vacuum level in accordance with the energy band theory. The transmission probability of secondary electrons through the surface barrier can be calculated quantum mechanically as long as the inner SE distribution is known.

Contrast and Resolution of SE Images

In a scanning electron microscope, without energy and angular analysis of secondary electron signals it is the total SE yield which determines the secondary electron image contrast regardless of the origin of the secondary electron generation and emission processes. This complicates the image interpretation since there are many factors that affect the total SE yield in an electron microscope. In the following discussion, we consider only type I secondary electrons which are ultra-high resolution image formation signals.

Contrast

By far the most striking features displayed in a secondary electron micrograph is that of the topographic contrast of specimen surfaces due to differences in path lengths of primary electrons close to the surface from which the generated secondary electrons can escape. This is the basis of high resolution imaging of surface topography by secondary electron signals. As an example demonstrating this image contrast figure 1 (a) shows a secondary electron image of the surface of a freshly crushed WO_3 crystal, revealing clearly the terrace structure of the fractured surface by topographic contrast. There exist very few steps on each flat terrace of the same crystallographic plane but complicated surface structures are revealed to exist at the transition region between two adjacent terraces as shown in figure 1 (b) which is a magnified image of the arrowed area in figure 1 (a). Figure 2 is a SE micrograph of ZnO smoke crystals revealing the crystal growth morphology clearly. The very bright area on the right hand side of the image is due to the fact that the incident beam makes small angles with two other long needles, giving very high total SE yield due to the large primary beam path length along the edges of the crystal. The contrast of these images may not be difficult to explain and they show the power of secondary electron imaging study of surface steps.

Various contrast mechanisms obtainable with detection of SE signals in a STEM instrument have been previously described [32]. Adsorption and contamination on specimen surfaces will inevitably change SE image contrast by change of transition probability via change of work function or surface states (monolayer adsorption) or by change of original generation and diffusion processes of SE signals (thick contamination layers). Oxidation of surface layers usually increases the total SE yield. The increase of SE signal of silicon crystals under electron beam irradiation could be due to the formation of thin oxide layers on the sample surface. On the other hand, under electron beam irradiation the decrease of SE signal of contaminated aluminum crystals is the result of the build-up of carbon layers and the subsequent formation of polymerized carbonaceous materials which decrease the total SE yield. The change of SE signal of MgO crystals under electron beam irradiation due to monolayer coverage of carbon material has been reported [11, 31-32].

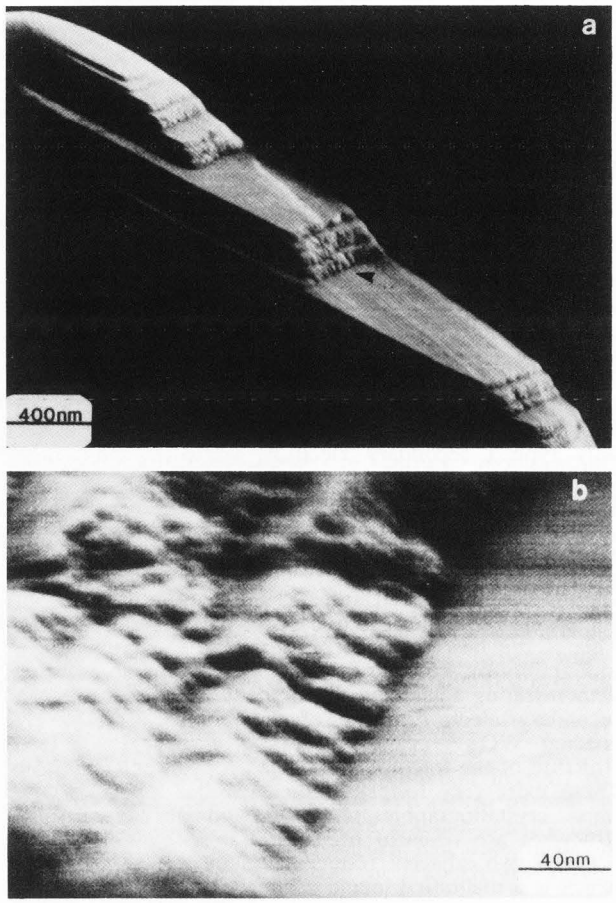

FIGURE 1: Secondary electron micrographs of surface terraces and steps of a crushed WO_3 crystal. (a) low magnification image showing the flat terraces and (b) magnified image of the arrowed area in (a) revealing the complex surface structures on this transition region.

The thickness dependence contrast of SE images of insulators and semiconductors, obtained in a STEM instrument [32] can be tentatively explained in light of the origin of SE emission discussed in the last section. For thin specimens ($<$ 5 nm) the cascade electrons may be negligible. The collected SE signals are produced directly by incident electrons and they are the coherently emitted secondary electrons as defined above. These electrons are real secondary electrons in the sense that they are generated directly by incident electrons and have suffered no inelastic scattering before they escape. These electrons may give higher resolution imaging signals than any other secondary signals. As the specimen thickness increases the cascade electrons make larger and larger contributions to the total image forming signal. Thus the SE image intensity will increase with thickness. At a certain thickness t_c the maximum yield is reached and then the total yield will decrease slowly with thickness. Another contribution to this change of intensity is that the mean free path of low energy secondary electrons is very large for insulators (most common ones are metal oxides). Secondary electrons of energies less than 2 E

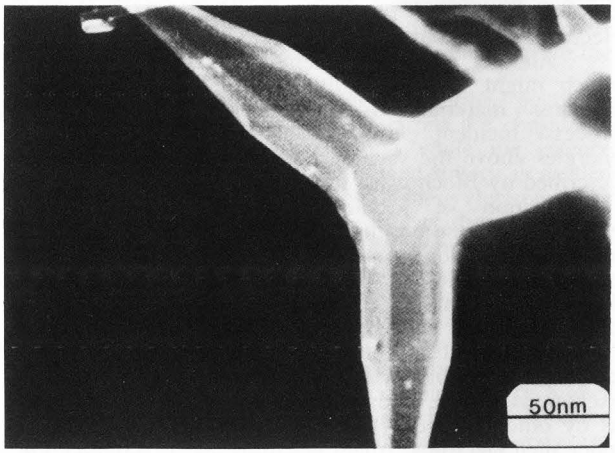

Figure 2: SE image of a ZnO smoke crystal showing the growth morphology clearly. Notice the very high intensity on the right hand side of the image (see text for discussion).

(E is the energy gap between valence band and conduction band) cannot be inelastically scattered by other specimen electrons since they do not have enough energy to excite the specimen electrons to conduction bands. Thus these low energy secondary electrons have a very low inelastic scattering probability on their way to the specimen surface, and so have a large inelastic mean free path. Thus as the specimen thickness increases more secondary electrons are generated inside the specimen and they can escape because of a large mean free path. This results in the increase of SE signal with thickness. The last model can also partially explain the striking differences of the total SE yield between insulators and metals. Another factor contributing to the high SE yield of metal oxides may be that there exist internal fields in these ionic crystals which will more or less influence the total SE yield.

The total SE yield depends basically on three steps, which are (1) generation of SE; (2) diffusion to the surface; and (3) transmission through the surface barrier. Consequently SE image interpretation is difficult. The first two steps are intrinsic properties of the electron beam interaction with specific materials and they are insensitive to surface conditions. The third step can be easily influenced by external factors such as adsorption and thin layer contamination on specimen surfaces. A change in any step will induce a change of the total SE yield. In the following we consider two cases of SE imaging study of GaAs crystals to show the complexity of image interpretation.

Freshly crushed GaAs crystals supported on carbon film can be evaporated and re-deposited on the supporting film under electron beam irradiation in a STEM instrument with a chamber vacuum pressure about 5×10^{-9} Torr. These crystal surfaces may be considered to be clean immediately after the evaporation-deposition process. Figure 3 (a) is a secondary electron image of these re-deposited particles showing the general features of these small particles. Figure 3 (b) is a magnified image of part of the area shown in figure 3 (a). The

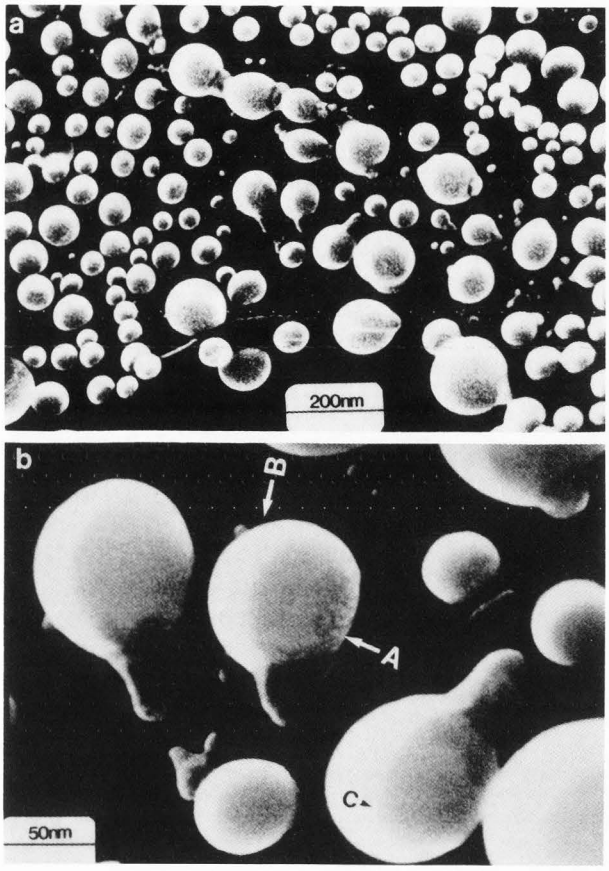

Figure 3: SE images of re-deposited GaAs particles. (a) low magnification image showing the general features of these small particles and (b) magnified image revealing the change of contrast from (A) (crystal) to (B) (amorphous) and the interface C between the two phases.

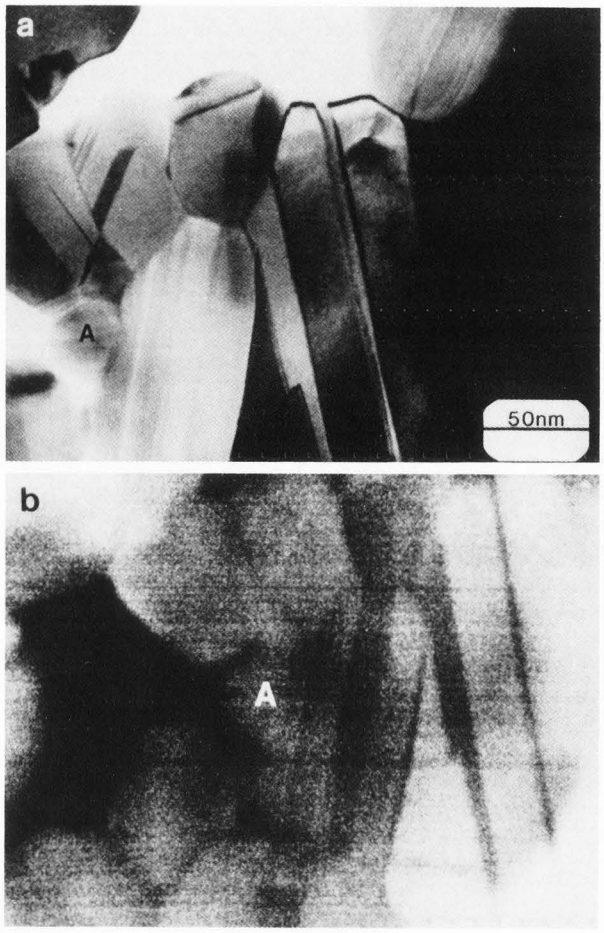

Figure 4: Twins of recrystallized GaAs crystals. (a) STEM image showing twins and (b) SE image revealing the same twins as in (a) with high contrast. The letter "A" indicates the same position on the two images.

contrast changes within the same particle from A to B as arrowed in the micrograph. Microdiffraction patterns show that part A is a crystal while part B gives diffraction patterns representing amorphous material. The contrast changes at the interface (arrowed as C) between the recrystallized GaAs and the amorphous GaAs. It seems that the amorphous part gives higher SE yield which may be due to the higher probability of producing secondary electrons for amorphous material than for crystals. Another complicating factor is the change of stoichiometry which also influences the total SE yield. Thus we need more information about the sample, which may be provided by other imaging or analytical modes in a STEM instrument, to interpret the secondary electron image contrast. Figure 4 (a) is a bright field STEM image of recrystallized GaAs crystals with various kinds of twins formed. These twins can also be imaged by secondary electron signals with high contrast as shown in figure 4 (b). Again the interpretation of this contrast is not a simple one. Channelling effects can be ruled out since channelling will not yield such high contrast images for type I secondary electron signals in a STEM instrument as discussed below. One possible explanation may be that the two twin planes have different atomic species on the top-most surface layer (e.g., one plane is Ga rich while the other plane is As rich). Another possibility is a preferential monolayer adsorption of gas molecules or less than a monolayer carbon contamination on one surface plane. Both of these two models can explain the observed SE image contrast as the result of change of work function from one atomic plane to the other. The twin contrast decreases with irradiation time as a result of the build-up of a thick layer of contamination. It may be noted that not all features in the STEM image give corresponding contrast in the SE image. These two examples raise the problem of how to interpret secondary electron images correctly. More information is needed in order to explain SE image contrast unambiguously. Other possible modes such as microdiffraction, electron energy loss analysis, secondary electron energy analysis and Auger electron analysis of surface composition can provide valuable information for the interpretation of SE images. Ultra-high vacuum is indispensable to maintain clean surfaces and may eliminate some uncertainties in the image interpretation.

Channeling effects have been observed in many fields in electron microscopy and diffraction [19, 37, 50-51]. A simple model to explain this is that the

strength of the electron beam-specimen interaction depends on the beam-specimen orientation relationship. At certain incidence angles, the primary beam will pass between the rows of atoms along channels. For other incident angles, the incident beam will interact more strongly with the specimen atoms. A more rigorous description of this phenomenon uses the Bloch wave model to describe the various properties of high energy electrons in a crystal. In the simple two-beam dynamical diffraction case, at any incident orientation the properties of fast electrons can be represented by a superposition of two types of Bloch waves, namely type I waves (weakly coupled with the atoms and travelling along channels between atom rows) and type II waves (strongly interacting with the atoms). The probability of exciting each wave differs as a function of the beam-crystal orientation. For incident angles less than a corresponding Bragg angle θ , the type II Bloch wave will be strongly excited and the incident electrons travel close to the atoms which results in large inelastic scattering cross-sections and consequently high yields of ionization products. For other cases, the type I Bloch waves dominate and electrons travel deep inside the crystal without experiencing significant energy loss. Thus less secondary products are produced at the entrance face but more may be produced at the exit face of a thick crystal. Channeling effects are expected for various kinds of secondary signals such as generation of X-rays, Auger electrons, cathodoluminescence and low energy secondary electrons, but may be obscured by multiple inelastic scattering effects. Channeling contrast of SE images is a form of emission number contrast. Channeling contrast has been observed in conventional SEM [36].

In a STEM instrument with SE signals detected at the exit surface the condition for detecting channeling contrast is different from that discussed above. For thin specimens ($<$ 5 nm) the channeling signal is too weak to be detected. For thick specimens, the channeling condition of the incident beam is destroyed at the exit surface due to elastic and inelastic scattering of the incident beam. Another disadvantage for detecting channeling contrast in this case is the incident beam convergence which will more or less smear out the channeling signal for SE imaging (e.g., at bend contours). As an example figure 5 (a) is a defocused bright field STEM image of a single silicon crystal with a micro-crack, showing the bend contours around the crack due to the bending of the crystal. Figure 5 (b) is the corresponding secondary electron micrograph of the same area, which does not reveal observable channeling contrast but the detailed topography around the crack. Experiments performed on thick specimens and other materials (e.g., standard stainless steel) indicate that it is hard to obtain an observable channeling contrast SE image. From the point of channeling phenomenon there is a difference between type I SE signals emitted at the entrance surface and that at the exit surface.

There is, however, another mechanism of generating channeling signals, which may be observable on a SE image. When the incident beam satisfies the condition for which the type II Bloch waves are strongly excited, the production of X-rays as well as energetic secondary electrons (inner shell electrons, Auger electrons, etc.) will be strongly enhanced. These ejected energetic secondaries will consequently produce more secondary electrons on their way to the surface and thus more secondary electrons will be detected. Similarly less

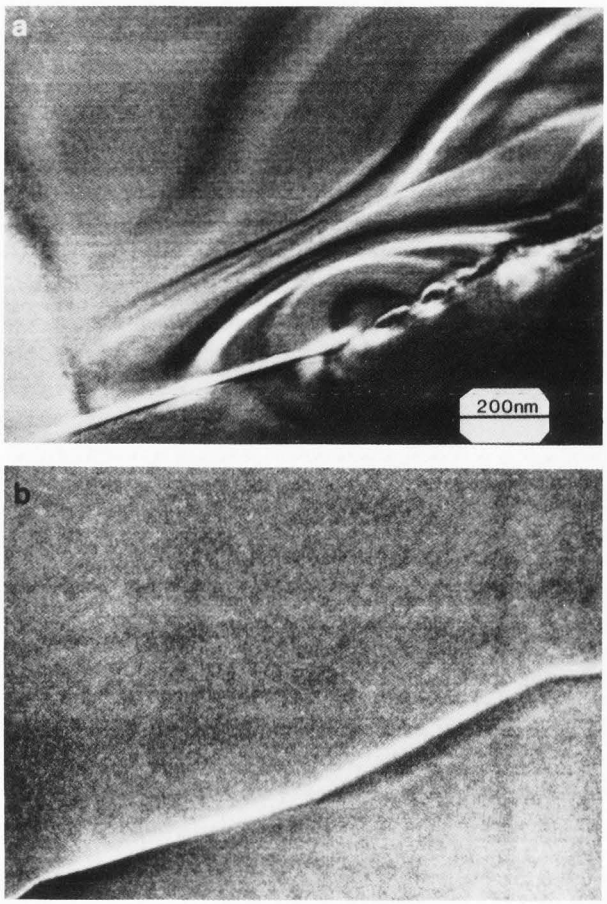

Figure 5: Bend contours of silicon crystal. (a) defocused STEM image revealing the various bend contours around a micro-crack and (b) the corresponding SE image showing the topography around the crack. There is no observable channeling contrast in the SE image.

secondary electrons will be collected for conditions of which type I Bloch wave is strongly excited. From this point of view bend contours can be imaged by secondary electron signals for thick specimens [3]. In order to have channeling effects for ionization products the inelastic excitation has to be localized within a distance (L) less than the corresponding lattice distance (d). This imposes a serious restriction on the energy of the ejected secondary electrons, which can produce the channeling contrast, from Heisenberg's Uncertainty Principle. Since the probability of generating high energy secondary electrons is small the channeling contrast of secondary electron images due to this generation mechanism, if observable, is very low.

Resolution

The resolution of secondary electron images can never be greater than that given by the probe size. Yet, this is not the only factor that determines the ultimate resolution limit of SE images. Generally three parameters determine the resolution of secondary electron images: (1) electron probe size; (2) signal to noise ratio and (3) range of electron beam-specimen interaction (spatial

distribution of generated secondary electrons). For low resolution images in a conventional scanning electron microscope the size of the electron probe is the key factor which determines the resolution. The localization of the spatial distribution of the generated secondary electrons will not affect the SE image resolution significantly. On the other hand, for ultra-high resolution SE imaging with a probe size of less than one nanometer in diameter it is the parameters (2) and (3) mentioned above which turn out to be the important factors in determining the ultimate resolution limit. These two parameters are also material dependent. Thus unlike the low resolution case the ultra-high resolution limit of a SE image depends on the specific material studied. Contrast and resolution are interrelated. High contrast usually accompanies high resolution for scanned images. The signal-to-noise ratio can be improved by using high brightness field emission guns. The problems involving the improvement of factors (1) and (2) mentioned above have been reported [13]. In the following we concentrate on the discussion of the physics of the electron beam-specimen interaction which determines the lateral spatial extent of the emitted secondary electrons.

As we discussed in the last section, the generation of secondary electrons is a result of inelastic scattering of incident electrons and the total yield is related to the total inelastic scattering cross-section. The inelastic scattering is delocalized. To first order approximation, we can take the spatial extent of the generated secondary electrons as proportional to the localization range L of the inelastic excitation processes. This problem has been studied by various authors [2, 12, 18, 20, 22, 24, 26, 38, 42, 48-49] working with the theory of image formation by inelastically scattered electrons and microanalysis in transmission electron microscopy (TEM) and STEM instruments. The generally accepted argument of the localization of an inelastic scattering event is based on Heisenberg's Uncertainty Principle and the idea of minimum momentum transfer **q** during the inelastic scattering event. The value of q, corresponding to zero-angle inelastic scattering of incident electrons, can be calculated from energy and momentum conservation of incident fast electrons with energy loss ΔE:

$$\mathbf{q} = \mathbf{K}(E) - \mathbf{K}(E-\Delta E) \qquad (2)$$

where $\mathbf{K}(E)$ and $\mathbf{K}(E-\Delta E)$ are the wave vectors of incident electrons before and after the inelastic scattering event, respectively, and E is the incident electron energy. For non-relativistic case and $\Delta E << E$:

$$q_{min} \simeq \sqrt{\frac{m}{2h^2}} \times \frac{\Delta E}{E^{1/2}} = \frac{\Delta E}{hV} = \frac{\pi \Delta E}{\lambda E} \qquad (3)$$

where V and λ are the incident electron velocity and wave length, respectively. From Heisenberg's Uncertainty Principle, we obtain the localization range L:

$$L \sim \lambda E/\Delta E \qquad (4)$$

Other estimates give approximately the same result [49]. With 100 keV electrons we have $L \simeq (400/\Delta E)$ nm where ΔE is in electron volts. For inner shell energy losses $\Delta E \sim 2$ keV, thus $L \leq 0.2$ nm, which can be considered to be localized excitations. On the other hand for valence electron excitation an average energy loss $\Delta E \sim 25$ eV is a good approximation. Thus the delocalized range of valence electron excitation is about $L \sim 15$ nm. In view of this estimate, the generated secondary electrons cannot be localized better than 15 nm for 100 keV electrons. This estimate is much larger than the experimental results (see below). The problems and refinements of the estimation of this localization range will be discussed in the next section.

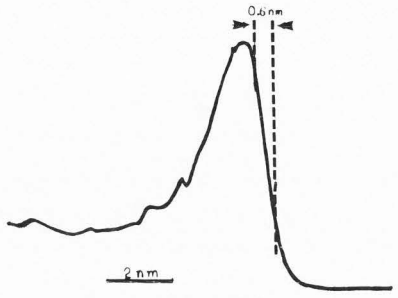

Figure 6: Line scan of SE signal across a straight edge of a very thin MoO_3 smoke crystal. The edge resolution in this image is about 0.6 nm.

Resolution of SE images in a STEM instrument generally depends on the localization range and signal to noise ratio since an electron probe as small as 0.5 nm or less is usually used. The image localization depends on the specific model of the excitation processes. For valence electron excitations the above estimate may not be valid since these electrons are initially delocalized. All inelastic scattering events contribute to the generation of secondary electrons. Large angle inelastic scattering excitation is more localized. Thus in practice, for a point incident beam it is the position and the half width of the intensity peak of the spatial distribution of the emitted secondary electrons that determines the experimental image resolution provided that the peak to background ratio is high enough. Experimental results have shown better localization than the theoretically estimated value. Figure 6 is a high magnification line scan of SE signal across the straight edge of a very thin MoO_3 smoke crystal prepared by burning Mo wire in air and collecting the smoke on a carbon coated copper grid. We estimated that the edge resolution of this image is about 0.6 nm which is of the order of the probe size. MoO_3 smoke crystals have a very high SE yield and they are always formed as regular thin sheets with straight edges, providing a good resolution test sample.

MoO_3 smoke crystals can be reduced to lower oxides and ultimately to Mo metal under electron beam irradiation. The reduction processes and the identification of the new products will be reported elsewhere (in preparation). The final product of this reduction process is molybdenum metal. Figure 7 is a secondary electron micrograph of the Mo crystals reduced from MoO_3 single crystal after a prolonged electron beam irradiation in a STEM instrument with a vacuum pressure of about 5×10^{-9} Torr. The small dark spots (0.5-3 nm) are Mo metal particles (sometimes conductive metallic oxides such as MoO, etc.) which are formed uniformly and

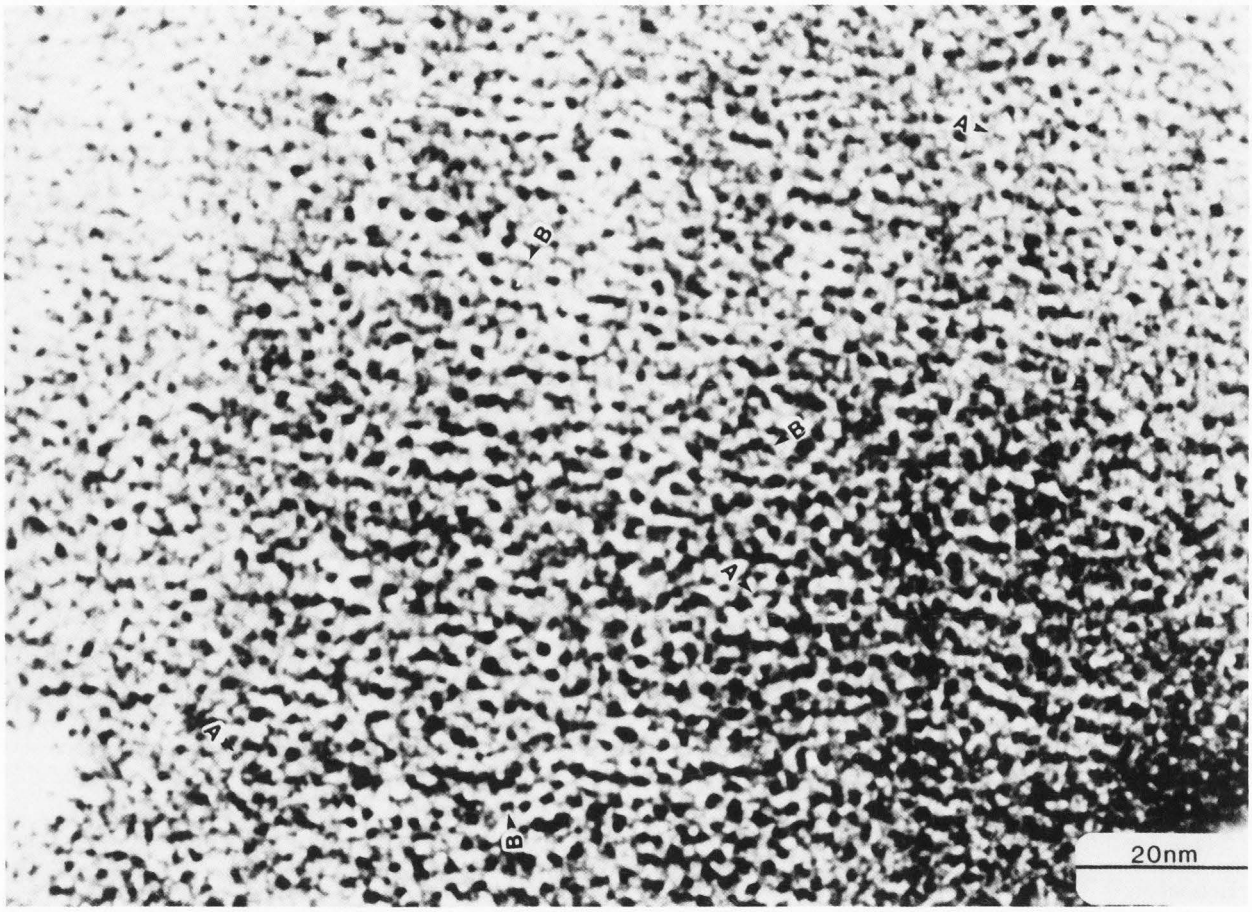

Figure 7: SE image of Mo metal particles reduced on a MoO_3 smoke crystal under electron beam irradiation. Small particles about 0.6 nm or less in diameter have been revealed (arrowed as A) and particle to particle distances as small as 0.7 nm have also been resolved in this image (arrowed as B).

epitaxially on the substrate as determined by microdiffraction patterns. Small particles about 0.7 nm in diameter have been revealed clearly (arrowed as A) and center to center distances of 0.7 nm between two small particles have also been resolved (arrowed as B). The resolution of secondary electron images revealed by this micrograph is better than 0.7 nm which is more than twenty times better than that estimated above. The high contrast of this image, which can be seen more clearly in figure 8, can be tentatively explained as follows. Metal oxides have very high SE yield as compared with conductive metals. The total SE yield of the system decreases with loss of oxygen atoms and at the same time the volume of the sample changes (becoming smaller). After long time irradiation, small particles of Mo metal, which give low SE yield, are formed and appeared dark on the SE image. The bright areas (arrowed as C) on the image are probably due to amorphous oxides (microdiffraction patterns have shown that there is amorphous materials overlapping on Mo particles) or due to the residual oxygen atoms or ions adsorbed on the surface which give high SE yield. There is another contribution to this surprisingly high contrast which is due to the geometric factor. These reduced Mo particles may shrink into the substrate due to the volume change, giving nanometer size "hills and valleys". This gives an additional dark-white contrast which coincides with the contrast due to other mechanisms. It is interesting to note that these metallic crystals are uniformly distributed (except for some degree of alignment in one direction which may be due to the preferential reduction of MoO_3 along the shear planes existing in MoO_3 crystals under electron beam irradiation) and are approximately in the same orientation except, in some cases for an azimuthal rotation of about 5 to 15 degrees with each other. Further electron beam irradiation will destroy this orientation relationship and then the small particles are randomly oriented.

Discussion

The intensity of the SE signal depends on the total number of secondary electrons generated, and escaping from the crystal, for the given incident beam position. The resolution of the image depends on the rate at which the signal changes as the probe is moved, and this

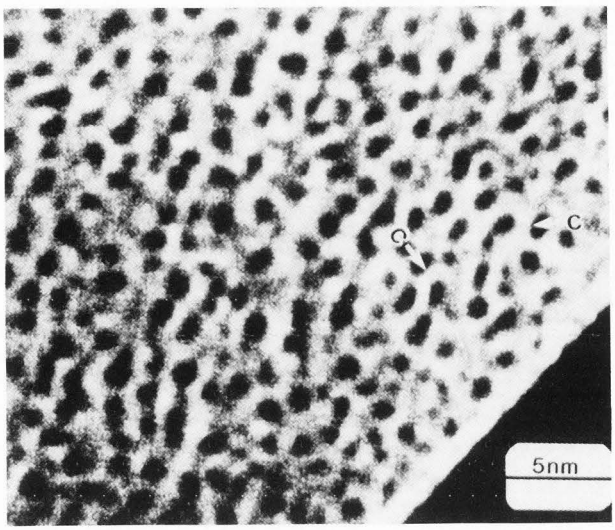

Figure 8: High magnification SE image of Mo metal particles on a reduced MoO_3 crystal showing the very high contrast. The very bright areas (arrowed as C) may be due to the adsorption of oxygen atoms/ions on the specimen surface which will give high SE yield. It is also possible that the bright areas represent a thin layer of amorphous oxides which have high SE yield.

depends primarily on the change in the number of primary inelastic scattering processes. The change in number of inelastic scattering processes determines the resolution of the energy-loss image obtained when all inelastically scattered electrons are collected. Resolution of secondary electron images is related to the localization of inelastic scattering excitations in a solid in the same way as for energy-loss images for this case. Experimentally obtained results as shown above cannot be simply explained by equation (4). In fact this estimation is based on the minimum momentum transfer along the incident beam direction which is irrelevant to the lateral spatial distribution of generated secondaries. **It is the higher-angle inelastic scattering that gives the highest resolution imaging signal.** If the inelastic scattering is taken to be confined to a cone of semi-angle Θ (characteristic inelastic scattering angle $\Theta = \Delta E/(2E)$), then the transverse localization is simply given by:

$$L = \lambda E/\Delta E \qquad (5)$$

which is the same as equation (4) but with different meaning.

Kohl and Rose [26] have calculated the image intensity profile of an atom formed by inelastically scattered electrons. The results indicate that for low energy losses the central sharp peak (which contains most of the total intensity) has a half width as well as a total intensity which are insensitive to the energy loss ΔE of the collected electrons. This means that for low energy excitations most of the inelastic scattering is localized within a small region L and this peak is superimposed on a broad low intensity background. The value of L will not change significantly with energy loss ΔE provided ΔE is less than a critical value ΔE_c depending on specific material. L can be evaluated by:

$$L = \lambda E/\Delta E_c \qquad (6)$$

Furthermore, large angle inelastic scattering events are more localized. For example at median scattering angle Θ which is defined such that half of the scattering occurs at angles larger than Θ and for typical materials $\Theta \simeq 10\,\Theta$ [15] for valence electron excitations. Hence, half of the inelastic scattering is localized within a region L:

$$L \sim \lambda E/(10\Delta E) \qquad (7)$$

By taking into account of these two factors we may conclude that most of the valence electron excitations are localized within a region L and the rest contribute a long tail to the intensity profile:

$$L = \beta\lambda E/\Delta E \qquad (8)$$

where β is a parameter depending on energy loss ΔE and the material studied. For 100 keV incident electrons this gives:

$$L \simeq (4\beta/\Delta E)\times 10^2 \text{ nm} \qquad (9)$$

where ΔE is in electron volts.

The production of secondary electrons depends on the total inelastic scattering cross-section. To first order approximation we can assume that the spatial intensity distribution of the generated secondary electrons is proportional to that of the inelastic scattering of incident electrons. Thus the localization of the secondary electrons immediately after its production can be taken as:

$$L = (4\beta/\Delta E)\times 10^2 \text{ nm} \qquad (10)$$

As a rough estimate of the localization effect we take $\Delta E = 25$ eV as an average energy needed to generate a secondary electron and $\beta = 0.05$ (corresponding to $\Delta E = 2\Delta E$), then L ~ 1 nm. This means that more than half of the generated secondary electrons are confined within this region for point incident electrons. The rest of the created secondary electrons forms a spatially extended background. Even this optimistic estimate cannot explain the experimental resolution approaching the beam size of 0.5 nm. Further knowledge of the spatial distribution of secondary electrons is needed.

More accurate estimates of the localization range should include the screening effect of the pulse electric field, produced by the incident fast electrons, by the specimen electrons in a solid. The screening length determines the range of the effective field which is related to the localization of the inelastic scattering. The screening effect will be larger for smaller angle scattering and lower energy losses. Hence, the localization of the generated secondary electrons will be much stronger for low energy secondary electrons than discussed above due to this screening effect. High resolution SE images can also be obtained by collecting these low energy secondary signals. For valence electron excitations plasmon excitation may play an important role for small angle scattering processes while single electron excitation will dominate for relatively large angle scattering processes. From the above discussion we know that larger angle scattering is more localized. **Thus the ultra-high resolution signals are mainly created through single electron excitation processes.** High energy

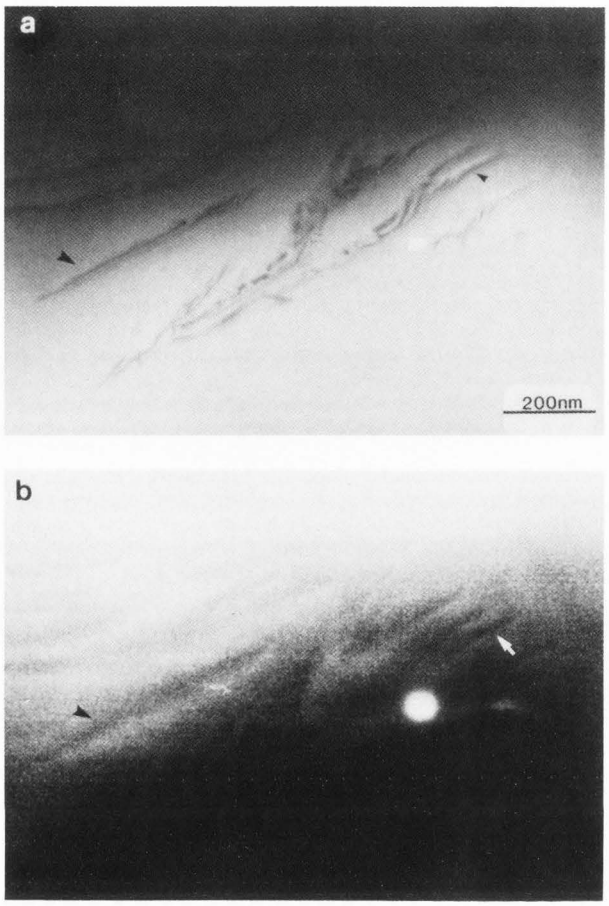

Figure 9: STEM image of a single silicon crystal with defects (a) and the corresponding SE image (b). The bright spot is the marker used for comparing the two images. The arrows indicate the same defects appearing in the two images. Compare the contrast and the shape of the defects in the two images.

secondary electrons (E > 100 eV) are certainly more localized and contribute to the ultra-high resolution signals. The collected SE signals depend on the total number of the secondary electrons produced and the resolution of SE images depends on how quickly this number changes at a discontinuity as the probing beam is scanned across the sample. Since the intensity distribution of the secondary electrons consists of a very sharp peak superimposed on a broad background, it is the specific shape and position of this central sharp peak which determines the experimentally obtained resolution limit.

Another interesting point to be noticed is that for thicker specimens the generation of cascade electrons by energetic secondaries may not degrade the resolution. In fact the production of energetic secondaries is quite well localized in view of equation (5) and this can give rapid changes of the secondary electron signal as the incident beam is moved. The subsequent generation of low energy electrons by these secondaries can be considered to contribute to a low-resolution background. The diffusion

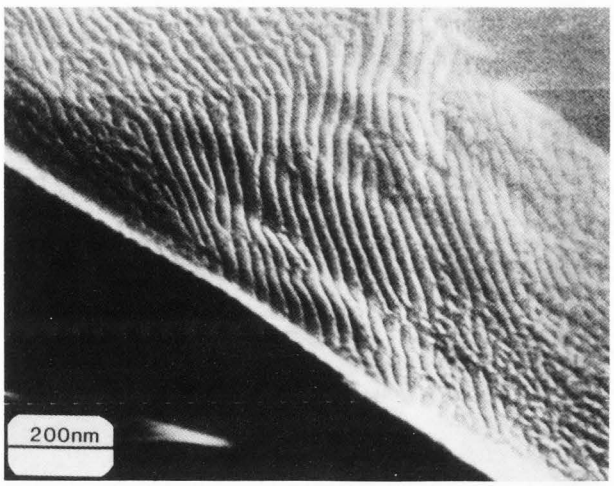

Figure 10: SE image of surface steps on a single silicon crystal. Note the roughness of the specimen surface.

broadening effect is the main factor responsible for the image resolution deterioration as the thickness increases.

Without energy analysis of secondary signals and better characterization of surface conditions the interpretation of SE image contrast can be very complicated in some cases. Figure 9 (a) is a BF STEM image of a silicon crystal showing some defects. Figure 9 (b) is the corresponding SE image (bright spot is the marker used to compare the two images) revealing the same defects with observable contrast. This contrast could be due to differences in SE yield of the defect region near the specimen surface or alternatively it may be due to preferential adsorption or contamination on the surface defects. More work is under way to investigate the correlation between surface defects and the change of SE signals. With energy analysis of the collected secondary electrons it may be possible to image surface defects by SE signals provided we have a very bright electron beam source. SE imaging of surface defects could be a valuable technique for materials science research.

SE imaging study of surface steps and surface morphology has been carried out [32]. The advantage over the Reflection Electron Microscopy (REM) study of surfaces is that this imaging technique can be used to study rough as well as flat surfaces of large and small crystals. Figure 10 is a secondary electron micrograph of surface steps on a crushed silicon crystal. This kind of surface cannot be imaged by REM and Scanning Reflection Electron Microscopy (SREM) techniques because of the roughness. Further work of SE imaging of flat surfaces (e.g., cleaved GaAs crystal surfaces) will be combined with SREM mode to extract more information about surface steps and to obtain better understanding of the contrast mechanisms of SE and SREM images.

It should be emphasized that combinations of several modes in a STEM instrument can give more, and more accurate, understanding of the studied material. Comparison of SE images with STEM energy loss images may yield information of the SE emission processes as well as the study of escape depths of various materials [21]. But the correlation between the two images is complicated. Energy loss images are usually

obtained by detecting small angle scattered incident electrons with an appropriate energy window. Secondary electrons are produced by all inelastic scattering events. The ultra-high resolution signals are generated by large angle inelastic scattering processes. More information about the SE generation mechanisms can be obtained by comparing the energy loss images, obtained by collecting all inelastically scattered electrons within a certain energy loss range, with the corresponding SE images. Comparison of SREM and SE images may reveal three dimensional features of the observed surface steps. Combination of microdiffraction technique with SE imaging proves to be a powerful method to study surface reactions under electron beam irradiation.

The contrast of secondary electron images is a purely emission-number contrast or amplitude contrast in the sense that there is no phase problem involved in the image formation. This simplifies the image interpretation as compared with TEM and STEM images. SE image is a direct magnified map of specimen surfaces (both electronic and geometric features) provided that the emission processes and the factors affecting the total SE yield are well understood.

With the new scanning transmission electron microscope, equipped with secondary electron energy spectrometer, Auger electron analysis and ultra-high vacuum chamber [55] we may extract more information about SE emission mechanism, give better interpretation of SE images and probably make further improvements in resolution of SE images by using energy filtered secondary electron signals.

Conclusion

Ultra-high resolution secondary electron imaging theory is far from complete. More knowledge of the secondary electron emission processes is needed in order to explain various experimental results. The study of the localization problem of inelastic scattering is the first step to the understanding of lateral spatial distribution of generated secondaries which determines the ultimate resolution limit of SE images.

In this paper, a resolution of SE images approaching the probe size of 0.5 nm has been demonstrated with a 100 keV STEM instrument. This resolution is much better than the theoretically estimated value for the localization of inelastic scattering excitations.

SE imaging can provide surface and subsurface information with subnanometer resolution but image interpretation can be very complicated for poorly characterized surfaces. With energy analysis of secondary signals in future ultra-high vacuum electron microscope, SE imaging will be a powerful tool in studying surface steps, surface reactions and other related surface problems.

Acknowledgements

This work was supported by the NSF grant DMR 8510059 and made use of the resources of the Facility for High Resolution Electron Microscopy, supported by the NSF grant 8306501.

References

[1]. Austin L, Starke H (1902). Ueber die Reflexion der Kathodenstrahlen und eine damit verbundene neue Erscheinung secundarer Emission. Ann. Physik 9, 271-292.

[2]. Batson PE (1981). Spatial resolution of plasmon scattering by high energy electrons. Analytical Electron Microscopy (1981),(ed) R. H. Geiss, San Francisco Press, San Francisco, 187-190.

[3]. Berger SD, Imeson D, Milne RH, McMullan D (1985). High resolution secondary electron imaging in a VG HB 501 STEM. Inst. Phys. Conf. Ser. No. 78, 99-102.

[4]. Bindi R, Lanteri H, Rostaing P (1980). A new approach and resolution method of the Boltzmann equation applied to secondary electron emission, by reflection from polycrystalline aluminium. J. Phys. D: Appl. Phys. 13, 267-280.

[5]. Bindi R, Lanteri H, Rostaing P (1987). Secondary electron emission induced by electron bombardment of polycrystalline metallic targets. Scanning Microsc. 1, 1475-1490.

[6]. Boiziau C, Gautier M (1984). Secondary electron emission: the place of the electronic structure. Scanning Electron Microsc. 1984; IV: 1665-1674.

[7]. Boiziau C, Leroy S , Perreau J, Reynaud C, Lecayon G, Le Gressus C (1985). Secondary electron emission through Auger relaxation of positive charges induced on an organic polymer. Scanning Electron Microsc. 1985; IV: 1385-1390.

[8]. Bronshtein IM , Denisov SS (1965). Study of secondary electron emission from solids with obliquely incident primary electrons. Soviet Physics-Solid State 7, 1484-1491.

[9]. Chung MS, Everhart TE (1974). Simple calculation of energy distribution of low energy secondary electrons emitted from metals under electron bombardment. J. Appl. Phys. 45, 707-709.

[10]. Chung MS, Everhart TE (1977). Role of plasmon decay in secondary electron emission in the nearly free electron metal-- application to Al. Phys. Rev. B, 15, 4699-4715.

[11]. Cowley JM, Glaisher R, Lin JA, Ou H-J (1986). Imaging and diffraction modes in scanning transmission electron microscopy. Proc. 44th Annual meeting EMSA, G.W. Bailey(ed). San Francisco Press, San Francisco. 684-687.

[12]. Craven AJ, Gibson JM, Howie A, Spalding DR (1978). Study of single-electron excitations by electron microscopy I. Image contrast from delocalized excitations. Phil. Mag. A, vol. 38, 519-527.

[13]. Crewe AV (1985). Towards the ultimate scanning electron microscope. Scanning Electron Microsc. 1985; II: 467-472.

[14]. Dekker AJ (1958). Secondary electron emission. Solid State Physics, vol. 6. Academic Press (New York). 251-311.

[15]. Egerton RF (1986). Chapter III; Electron Scattering Theory. Electron Energy Loss Spectroscopy in the Electron Microscope. Plenum Press (New York). 129-229.

[16]. Everhart TE, Chung MS (1972). Idealized spatial emission distribution of secondary electrons. J. Appl. Phys. 43, 3708-3711.

[17]. Hachenberg O, Bauer W (1959). Secondary electron emission from solids. Adv. Electronics and Electron Phys. 11, 413-499.

[18]. Howie A (1963). Inelastic scattering of electrons by crystals I. The theory of small-angle inelastic scattering. Proc. Roy. Soc. A, 271, 268-287.

[19]. Howie A (1966). Diffraction channelling of fast electrons and positrons in crystals. Phil. Mag. 14, 322-327.

[20]. Howie A (1981). Localization and momentum transfer in inelastic scattering. 39th Ann. Proc. Electron Microsc. Soc. Am.,(ed) G. W. Bailey, Claitor's Publishing, Baton Rouge, Louisiana, 186-189.

[21]. Howie A, Milne RH (1985). Excitations at interfaces and small particles. Ultramicroscopy 18, 427-434.

[22]. Humphreys CJ, Whelan MJ (1969). Inelastic scattering of fast electrons by crystals I. Single electron excitations. Phil. Mag. A, vol. 20, 165-172.

[23]. Imeson D, Milne RH, Berger SD, McMullan D (1985). Secondary electron detection in the scanning transmission electron microscope. Ultramicroscopy 17, 243-250.

[24]. Isaacson M, Langmore JP (1974). Determination of the non-localization of the inelastic scattering of electrons by electron microscopy. Optik, Vol. 41, 92-96.

[25]. Kanter H (1961). Energy dissipation and secondary electron emission in solids. Phys. Rev. 121, 677-681.

[26]. Kohl H, Rose H (1985). Theory of image formation by inelastically scattered electrons in the electron microscope. Advances in Electronics and Electron Physics. vol. 65. Academic Press (New York). 173-227.

[27]. Korablev VV, Kudinov YA, Sysoev SN (1986). Effect of the band structure of a solid on the spectrum of angular resolved secondary electron emission. Sov. Phys., Solid State 28, 1485-1489.

[28]. Korablev VV, Kudinov YA, Sysoev SN (1987). Calculated and experimental spectra of slow secondary electrons emitted at different angles to the (100) surface of tungsten. Sov. Phys., Solid State 29, 402-404.

[29]. Kuroda K, Hosoki S, Komoda T (1986). High resolution observation of field emitter tips with a SEM. Proc. 11th Int. Conf. Elec. Microsc., Kyoto. Publ. JEM. Tokyo, Japan. 277-278.

[30]. Kuroda K, Hosoki S, Komoda T (1987). Observation of tungsten field emitter tips with an ultra-high resolution field emission scanning electron microscope. Scanning Microsc. 1 , 911-917.

[31]. Liu J, Cowley JM (1987). High resolution SEM for surface reactions. Ultramicroscopy 23, 463-472.

[32]. Liu J, Cowley JM (1988). High resolution secondary electron imaging in a scanning transmission electron microscopy instrument. Scanning Microsc. 2, 64-78.

[33]. Nagatani T, Saito S (1986). Instrumentation for ultra high resolution scanning electron microscopy. Proc. 11th Int. Conf. Elec. Microsc. Kyoto. Publ. JEM. Tokyo, Japan. 2101-2104.

[34]. Nagatani T, Saito S, Sato M, Yamada M (1987). Development of an ultra-high resolution scanning electron microscope by means of a field emission source and in-lens system. Scanning Microsc. 1, 901-909.

[35]. Namba H, Murata Y (1984). Surface dislocation of MgO (100) studied by secondary electron emission spectroscopy and cathodoluminescence spectroscopy. J. Phys. Soc. Japan. 53, 1888-1898.

[36]. Newbury DE, Yakowitz H (1975). Chapter V; Contrast Mechanisms of Special Interest in Materials Science. Practical Scanning Electron Microscopy. (Eds), J. I. Goldstein and H. Yakowitz. Plenum Press (New York). 149-210.

[37]. Ohtsuki YH (1983). Charged beam interactions with solids. Taylor & Francis Ltd (London).

[38]. Pennycook SJ, Howie A (1980). Study of single-electron excitations by electron microscopy II. Cathodoluminescence image contrast from localized energy transfers. Phil. Mag. A, vol. 41, 809-827.

[39]. Reimer L (1979). Electron-specimen interactions. Scanning Electron Microsc. 1979; II: 111-123.

[40]. Reimer L, Drescher H (1977). Secondary electron emission of 10-100 kV electrons from ansparent films of Ag and Au. J. Phys. D: Appl. Phys., 10, 805-815.

[41]. Rosler M, Brauer W (1981). Theory of secondary electron emission. Phys. Status Solidi. B 104, 161-175, 575-587.

[42]. Rossouw CJ (1981). Localization effects in electron energy loss signals: Phenomena induced in characteristic loss rocking curves. Ultramicrosc. 7, 139-146.

[43]. Salehi M, Flinn EA (1980). An experimental assessment of proposed universal yield curves for secondary electron emission. J. Phys. D: Appl. Phys., 13, 281-289.

[44]. Schou J (1988). Secondary electron emisson from solids by electron and proton bombardment. Scanning Microsc. 2, 607-632.

[45]. Seah MP (1969). Slow electron scattering from metals. Surface Sci. 17, 132-213.

[46]. Seiler H (1983). Secondary electron emission in the scanning electron microscope. J. Appl. Phys. 54, R1-R18.

[47]. Sickafus EN (1977). Linearized secondary-electron cascades from the surfaces of metals. Phys. Rev. B; 16, 1436-1458.

[48]. Spence JCH (1981). The crystallographic information in localized characteristic loss electron images and diffraction patterns. Ultramicrosc. 7, 59-64.

[49]. Spence JCH (1988). Chapter VI; Inelastic Electron Scattering. High Resolution Transmission Electron Microscopy. P. R. Buseck,(ed), Oxford Univ. Press, Oxford.

[50]. Taftϕ J, Krivanek OL (1982). Site-specific valence determination by electron energy loss spectroscopy. Phys. Rev. Lett. 48, 560-563.

[51]. Taftϕ J, Lempfuhl G (1982). Direction dependence in electron energy-loss spectroscopy from single crystals. Ultramicrosc. 7, 287-294.

[52]. Tamura E (1985). On the theory of secondary electron emission. J. Phys. Soc. Japan, 54, 4631-4635.

[53]. Tanaka K, Matsui I, Kuroda K, Mitsushima A (1985). A new ultra-high resolution scanning electron microscope (UHS-T1). Biomedical SEM 14, 23-25.

[54]. Tanaka K, Mitsushima A, Kashima Y, Osatake H (1986). A new high resolution scanning electron microscope and its application to biological materials. Proc. 11th Int. Conf. Elec. Microsc., Kyoto,1986. Publ. JEM. Tokyo, Japan. 2097-2100.

[55]. Venables JA, Cowley JM, Von Harrach HS (1987). A field-emission STEM for surface studies. In Proc. EMAG conference, Institute of Physics, Conf. Ser. 90, 85-88.

Discussion With Reviewers

H. Seiler: I assume you use for your experiments a STEM with detection of the SE "through the lens", i.e. the SE spiral around the magnetic field lines and can emerge from the top of the lens to the SE-detector by an electrostatic field. So from the different SE-signals you can avoid the type III SE-signal (SE released at the walls of the object chamber by BSE) and type IV BSE-signal (BSE emitted in the direction of the collector). The type II SE-signal is negligible (SE released by BSE at the specimen surface) due to the very thin object. The "coherent SE" were detected in the spectrum of the angular resolved SEE. Do you think there is a certain energy filtering or an angular filtering characteristic in your detection system ?
Authors: Since the emitted secondary electrons experience a fringe magnetic field, which will focus secondary electrons to a small cone around the optic axis, before they are detected there is no sharp angular filtering in the detection system. Furthermore the spiraling secondary electrons are extracted to the SE detector from the optic axis by a deflection electrostatic field. The collection efficiency should be higher for low energy secondary electrons than that for high energy secondary electrons. Thus, there is some energy filtering effect in this sense.

H. Seiler: Can you give more information on the "coherent" SE. For S/N and contrast considerations the ratio of "coherent" SE to common SE is of special interest.
Authors: For 100 kV incident electrons, the coherent secondary electrons can be significant only for very thin specimens since these hot secondary electrons have a very short inelastic scattering mean free path. The ratio depends on the sample thickness. For a low energy incident beam ref. 3 has given some calculated and experimental results.

T. Nagatani: Your discussions on the contrast and resolution of SE images are confined only to type I signals. As you are no doubt aware that the type II (SE signals due to BSE), and even type III SE signals, significantly affect the SE contrast, it may be too unrealistic to apply the discussion on the SE images obtained. How do you estimate these effects on the SE image you have shown in the paper, especially for those shown in a comparative way with the STEM.
Authors: The text discussions all refer to high resolution signals (type I signals). At high magnification (corresponding to resolution about 1 nm) type II SE signals will only contribute a background intensity to the image, lowering the image contrast slightly. Type II SE signals will be important only for low resolution images which is not relevant to this paper. Furthermore, in our detection configuration type II secondary electrons are negligible. Type III SE signals are not significant for thin specimens. The contribution of type III signals will increase with specimen thickness. This will give extra thickness dependent contrast. These two types of signal have little effect on the SE images reported in this paper.

D. Imeson: Is it possible that the increasing SE signal with increasing thickness is due, at least in part, to an increasing contribution from secondaries produced subsequently from high angle scattered primaries impinging on parts of the specimen cartridge and microscope (i.e., "Type III" or "Type IV" secondaries)?
Authors: Yes, some contribution may come from these sources but they will not play a significant role for crystal thickness of 20 nm -- 200nm. These secondary electrons may produce an image contrast similar to large angle annular dark field images. These signals may also contribute to high resolution signals although they carry 'false' information.

H. Seiler: As shown by Venables and other authors the onset point of the energy distribution of the SE shifts with change of the work function. Moreover applying a negative potential of some 100 volts on the specimen sometimes allows imaging of submonolayers on surfaces in a SEM (biased SE-imaging, Venables and co-workers). Can these two effects contribute to the high resolution and contrast in your pictures ?
Authors: Change of work function should have a strong effect on the emission of low energy secondary electrons and the contrast of the SE image. Negative bias of the sample will increase the total SE signal due to the extraction field. This will enhance the contrast of the SE image. The two factors will not affect the SE image resolution significantly. We did not bias the sample in our experiment. Change of work function should contribute to the image contrast such as the one shown in figure 8.

H. Seiler: Can the contrast in Fig. 8 be explained by the position of the object details, i.e. can you observe a change in contrast by object rotation ?
Authors: MoO_3 smoke crystals are formed into thin sheets with thickness of about 10 nm to 50 nm. The crystal imaged in figure 8 was about 20 nm in thickness and the incident beam was along [010] direction. The contrast is due to change of work function, surface geometry and possibly some voltage difference between the reduced particle and the substrate. Object rotation did not change the contrast significantly except the increase of signal due to the increase of incident beam path length.

D. Imeson: I find it hard to believe your interpretation of figure 3 in terms of amorphous and crystalline GaAs. The images look to me as I would expect such particles to look purely because of edge effects. Do you have more evidence of the amorphous/crystalline interface such as obtained from bright field micrographs, suitably oriented so that the two regions are clearly imaged ?
Authors: There may be other possible interpretations of this image but the evidence for the crystalline-amorphous division is strong. It seems unlikely that edge effects are important because the secondary electron collection should be isotropic whereas some edges are bright, some are dark and the bright edges occur in various directions. Bright field STEM image did not give much information because the particles are very thick. Microdiffraction patterns did show the amorphous and crystalline parts of the particle. HRTEM observations of re-deposited GaAs particles in other cases have also confirmed that the small particles consists frequently of crystalline part (GaAs) and amorphous part. EELS study of these re-deposited particles indicated that the amorphous part may have different stoichiometry from GaAs (Wang, Materials Letters, Vol. 6; 1988. p112).

D. Imeson: In all your discussions of contrast you make no reference to the effects of specimen charging. In the experience of myself and colleagues this is a major factor - the secondary image is strongly affected by a small build up of charge, small enough to have no effect on the images formed by primary electrons, which will only respond to gross charging.

Authors: The effect of specimen charge-up upon SE signals is quite complicated. We mentioned this effect in our previous paper (Scanning Microsc. 2, 65-81). SE signals should be sensitive to any electric fields present at or around the irradiated area since they have low kinetic energies. The charging up of the specimen is generally not uniform. It depends on sample surface geometry (e.g., micro-protrusions and depressions, atomic steps on surfaces, etc.) and local conductivity of the sample. Non-uniform charge-up on the specimen surface will affect the contrast of high resolution SE images significantly. But there is no existing theory to incorporate this mechanism to explain the effect of the micro-charge-up of specimen surfaces on SE image contrast. Therefore this problem should be studied more systematically before any definite conclusion can be made.